Biochemical and Biophysical Research Communications 456 (2015) 403–409

Contents lists available at ScienceDirect

Biochemical and Biophysical Research Communications

journal homepage: www.elsevier.com/locate/ybbrc

Crystal structure and solution characterization of the thioredoxin-2 from *Plasmodium falciparum*, a constituent of an essential parasitic protein export complex

Mindy Peng [a], Duilio Cascio [b], Pascal F. Egea [a,c,*]

[a] Department of Biological Chemistry, David Geffen School of Medicine, UCLA, Los Angeles, USA
[b] Department of Energy Institute for Genomics and Proteomics, UCLA, Los Angeles, USA
[c] Molecular Biology Institute, UCLA, Los Angeles, CA, USA

ARTICLE INFO

Article history:
Received 28 October 2014
Available online 2 December 2014

Keywords:
Plasmodium falciparum
Protein translocon of exported proteins
Antimalarial design
Hybrid methods
Crystal structure
SAXS

ABSTRACT

Survival of the malaria parasite *Plasmodium falciparum* when it infects red blood cells depends upon its ability to export hundreds of its proteins beyond an encasing vacuole. Protein export is mediated by a parasite-derived protein complex, the *Plasmodium* translocon of exported proteins (PTEX), and requires unfolding of the different cargos prior to their translocation across the vacuolar membrane. Unfolding is performed by the AAA + protein unfoldase HSP101/ClpB2 and the thioredoxin-2 enzyme (TRX2). Protein trafficking is dramatically impaired in parasites with defective HSP101 or lacking TRX2. These two PTEX subunits drive export and are targets for the design of a novel class of antimalarials: protein export inhibitors. To rationalize inhibitor design, we solved the crystal structure of *Pfal*-TRX2 at 2.2-Å resolution. Within the asymmetric unit, the three different copies of this protein disulfide reductase sample its two redox catalytic states. Size exclusion chromatography and small-angle X-ray scattering (SAXS) analyses demonstrate that *Pfal*-TRX2 is monomeric in solution. A non-conserved N-terminal extension precedes the canonical thioredoxin-fold; although it is not observed in our structure, our solution analysis suggests it is flexible in contrast to *Plasmodium* thioredoxin-1. This represents a first step towards the reconstitution of the entire PTEX for mechanistic and structural studies.

1. Introduction

Malaria, an infectious disease cause by the parasite *Plasmodium*, is one of the first causes of mortality and morbidity worldwide. The major challenges posed by malaria are the emergence and spread of drug resistant-parasites combined to the relative poor chemical diversity of available drugs [1]. Until now the therapeutic arsenal consisted of drugs belonging to the quinoline and antifolate groups with the recent addition of artemisin-type compounds. To expand the repertoire of therapies, identification of new drug targets for the development of novel classes of antimalarial drugs remains a priority.

Plasmodium falciparum (*Pfal*) causes the most lethal form of malaria. Most of the pathological manifestations of the disease occur at the blood stage of the infection when this obligate intracellular parasite invades red blood cells. *Plasmodium* extensively remodels blood cells to multiply and evade the immune response. To survive within erythrocytes, the parasite exports hundreds of its proteins (~5–7% of its proteome) beyond an encasing parasitophorous vacuole (PV). Some 25% of the exported proteins are essential to the parasite survival and mediate its virulence [2–4]. A parasite-derived protein export complex, the *Plasmodium* translocon of exported proteins (PTEX), mediates this essential and extensive parasitic protein export [5] (Supplementary Fig. S1A). The PTEX is composed of 5 subunits: EXP2, HSP101/ClpB2, PTEX150, TRX2 and PTEX88 (Supplementary Fig. S1B). EXP2, PTEX150 and HSP101/ClpB2 components associate into a detergent-resistant core complex that can be extracted from parasites membranes [6]. The membrane-associated subunit EXP2 (exported protein-2) [7,8] is a possible candidate for the trans-membrane protein-conducting pore and may structurally resemble hemolysins, bacterial pore-forming cytolytic α-helical toxins [9–11]. Proteins destined for export harbor a vacuolar secretion signal or PEXEL (*Plasmodium* export element) [12,13]. Proteolytic processing of the PEXEL by the endoplasmic reticulum protease Plasmepsin V is necessary in order

* Corresponding author at: UCLA David Geffen School of Medicine, Department of Biological Chemistry, Boyer Hall room 356, 611 Charles E. Young Drive East, Los Angeles, CA 90095, USA.
E-mail address: pegea@mednet.ucla.edu (P.F. Egea).

http://dx.doi.org/10.1016/j.bbrc.2014.11.096
0006-291X/

to license the cargo proteins for export [14,15]. Protein export requires unfolding of the different cargos prior to their translocation across the PV membrane [16]. Unfolding is performed by HSP101/ClpB2, a ClpB AAA + protein [17] and is assisted by the thioredoxin-2, a protein-disulfide isomerase that reduces disulfide bonds of cargo proteins to facilitate export.

Repeated attempts to generate gene knockouts of any of the three PTEX components EXP2, PTEX150 and ClpB2/HSP101 initially failed [5], suggesting their essential functions as core components of the PTEX. Parasites deficient in PTEX150 or HSP101 have greatly reduced trafficking of all classes of exported proteins [18] beyond the enveloping vacuolar membrane. Even a modest knockdown of PTEX components has a strong effect on the parasite's ability to complete the erythrocytic stage of its lifecycle [19]. Mutant parasites lacking TRX2 or PTEX88 are severely impaired with considerably slower rates of development during the blood stage [20]. These studies have led to the conclusions that while EXP2, HSP101 and PTEX150 play central roles during the blood infection in *Plasmodium*, PTEX88 and TRX2 are auxiliary yet important regulators of PTEX-mediated protein export and required for maintaining normal blood-stage growth [21]. As HSP101/ClpB2 is the ATP-powered molecular motor driving protein export and TRX2 assists the unfolding process, there is a keen interest in designing inhibitors of these two proteins.

As an essential nexus for protein export in the malaria parasite, PTEX is a prime drug target. Small-molecule inhibitors of thioredoxins and ClpB AAA + proteins have been described and identified using high-throughput screening [22] and/or computational methods [23]. To this aim, we have characterized the solution and crystal structures of *P. falciparum* TRX2 to facilitate the rational design of inhibitors and gain mechanistic insights into the molecular mechanism of this essential parasitic protein export machine.

2. Materials and methods

2.1. Protein purification and crystallization

A synthetic codon-optimized gene encoding residues T23-L157 of *Pfal*-TRX2 (PF3D7_1345100) was designed for its expression in *Escherichia coli* as a C-terminal octa-histidine fusion protein (residues M1 through C22 correspond to the signal sequence) using the pJexp401 expression vector. The protein was expressed in C43(DE3) *E. coli* cells grown in LB media at 37 °C until they reached OD600 = 0.6 at which point protein expression was induced with 0.8 mM IPTG. Seleno-methionine-labeled *Pfal*-TRX2 was expressed in minimal media with glucose as carbon source and using the methionine pathway inhibition labeling method [24]. Cells were washed in 150 mM KCl and 20 mM Tris pH = 7.8, and stored at −80 °C until processing. Cells were lysed in 500 mM NaCl, 20 mM Tris pH = 7.8 and 15% glycerol supplemented with 2.8 mM β-mercaptoethanol (β-ME), 0.2 mM of phenylmethylsulfonyl fluoride (PMSF), and 1 tablet of EDTA-free protease inhibitor cocktail. Cells were disrupted by three passes through a C-3 Emulsiflex pressurized at 15,000 psi. The lysate was clarified by centrifugation at 25,000*g* for 1 h, after which the total soluble extract was applied onto a gravity-flow column packed with 5–10 mL of Cobalt-NTA IMAC resin. Non-specifically bound bacterial proteins were washed using Cobalt-A wash buffer (12.5 mM imidazole, 500 mM NaCl, 20 mM Tris pH = 7.8, 10% glycerol, 2.8 mM β-ME and 0.2 mM PMSF). The protein was eluted from the column with Cobalt-B buffer (125 mM imidazole, 500 mM NaCl, 20 mM Tris pH = 7.8, 10% glycerol, 2.8 mM β-ME and 0.2 mM PMSF). The IMAC eluate was desalted using a PD-10 desalting column equilibrated in 100 mM NaCl, 20 mM Tris pH = 7.8, 2% glycerol, 2.8 mM β-ME and 0.2 mM PMSF, to remove imidazole. Following desalting, the protein was purified by ion exchange chromatography on a CaptoS column. The sample was treated with thrombin for 24 h at 4 °C (0.25 units enzyme/mg of protein) to remove the histidine purification tag. Following thrombin treatment, the sample was further purified on a mixture of Nickel-NTA IMAC and Benzamidine Sepharose. The final purification step consisted in a size exclusion chromatography (SEC) on a Superdex 75 HR10/30 gel-filtration column equilibrated in 150 mM NaCl, 20 mM Tris pH = 7.8, 2% glycerol, and 7 mM β-ME to condition samples for crystallization trials (Supplementary Fig. S2).

High-throughput crystallization trials were performed with a robotic nanoliter Mosquito workstation in hanging-drop setups using the vapor diffusion technique at 4 °C. Suitable crystals grew in 10–15% isopropanol, 10–15% PEG 4000 and 100 mM Na-Citrate buffer at pH = 5.0 (Supplementary Fig. S2). Crystals of selenium-labeled protein grew in similar conditions.

2.2. Data collection, structure determination, and refinement

Diffraction data were collected on beamlines 24-ID-C or 24-ID-E at the Advanced Photon Source in the Argonne National Laboratory using crystals cryoprotected in mother liquor supplemented with 20–25% glycerol. Data were indexed, scaled and reduced using *XDS* [25].

The structure of *Pfal*-TRX2 was phased by the single anomalous dispersion method using the signal of selenium collected on a single crystal diffracting at 2.5 Å. A 2.2 Å resolution native diffraction data set was used for the final refinement. Phasing was performed with *HKL2MAP* with partial automatic building. Model building and refinement cycles were carried out in Coot [26] and *Phenix* [27] where the three *Pfal*-TRX2 molecules observed in the asymmetric

Table 1
X-ray diffraction data collection and structure refinement statistics.

Plasmodium-TRX2	PDB ID 4O32
Data set	APS 042311 24-ID-C
Data collection statistics	
Wavelength	0.97918 Å
Resolution (last shell)	50–2.20 Å (2.26–2.20 Å)
Unique reflections	21,285 (1486)
Completeness	96.6% (99.6%)
$I/\sigma(I)$	22.9 (3.2)
Redundancy	14.5 (13.6)
R_{sym}	4.7% (67.2%)
R_{meas}[a]	5.1% (72.8%)
$CC(1/2)$[b]	100% (87.7%)
Space group	$P4_32_12$
Unit cell dimensions	a = 77.4 Å, c = 134.8 Å
AU content	3 Molecules
Solvent content	61%
Refinement statistics	
Resolution	50–2.2 Å
Reflections	21,273
Work set/test set	20,181/1092
R_{free}/R_{cryst}	24.9%/20.7%
B_{wilson}	52.0 Å^2
Protein atoms, ADP	2184, 55.1 Å^2
Solvent atoms, ADP	71, 65.3 Å^2
Others atoms, ADP	1 Chloride, 40.1 Å^2
rmsd bonds	0.004 Å
rmsd angles	0.600°
Ramachandran analysis	
Allowed regions	96.7%
Generously allowed	3.3%
Outliers	0.5%

[a] R_{meas} is the redundancy independent *R*-factor [38].
[b] $CC(1/2)$ is the percentage of correlation between intensities from randomly selected half-datasets [39].

unit were refined independently without applying non-crystallographic symmetric restraints. Atomic displacement parameters (ADPs) were refined using the combination of individual isotropic and TLS strategies in *Phenix* (Table 1).

2.3. Small angle X-ray scattering measurement and data analysis

Solution scattering data were collected at the SIBYLS high-throughput SAXS beamline 12.3.1 [28] of the Advanced Light Source at the Lawrence Berkeley National Laboratory. Samples were further purified by gel filtration in the SAXS experimental buffer 200 mM NaCl, 20 mM Tris pH = 8.0, 2% glycerol, 0.5 mM EDTA and 5 mM fresh DTT with concentrations ranging from 1 to 25 mg/ml. All intensity curves were collected with a sample-to-detector distance of 1.5 m and an X-ray wavelength of $\lambda = 1$ Å and each contained about 500 data points. This corresponds to a Q ranging from 0.001 to 0.32 Å^{-1}, with Q the scattering vector defined as $Q = 4\pi\sin\theta/\lambda$ where 2θ and λ are the scattering angle and X-ray wavelength, respectively. For each sample several exposures were sequentially recorded (0.5, 1, 2 and 4 s). Corresponding to each protein sample, data were collected on a buffer sample under identical experimental conditions. A beamline specific software was used for radial averaging of images and for subtracting buffer signal from protein signal [29]. Each scattering profile was visually inspected to check for aggregation, repulsive or attractive interactions, X-ray induced damage, detector saturation or anomalies in buffer subtraction. Following data reduction, analysis of experimental scattering data was performed using *Scatter* (http://bl1231.als.lbl.gov/saxs_protocols/index.php and http://www.bioisis.net/) to determine the radius of gyration (R_G) by Guinier analysis, $P(r)$ and D_{max}. Kratky plots were used to assess the particle flexibility and folded nature [30]. Scattering curves corresponding to the X-ray structures reported in this study were calculated and fitted against the experimental scattering curves using CRYSOL [31] with default parameters; the discrepancy factor χ^2 was used to estimate the quality of the fits between experimental and calculated scattering curves. Pair distance distribution functions ($P(r)$) were derived by Fourier transform using *GNOM* [32] to estimate D_{max}, the longest distance occurring within the particle, and R_G, independently of Guinier analysis.

3. Results and discussion

3.1. Structure of the Plasmodium thioredoxin-2 and conformational variability of the N-termini in other Plasmodium thioredoxins

We solved the crystal structure of *Pfal*-TRX2 at 2.2 Å resolution using the anomalous dispersion signal of selenium (Table 1). This is the best resolution achieved for this specific thioredoxin so far; high-resolution crystal structures are better templates for

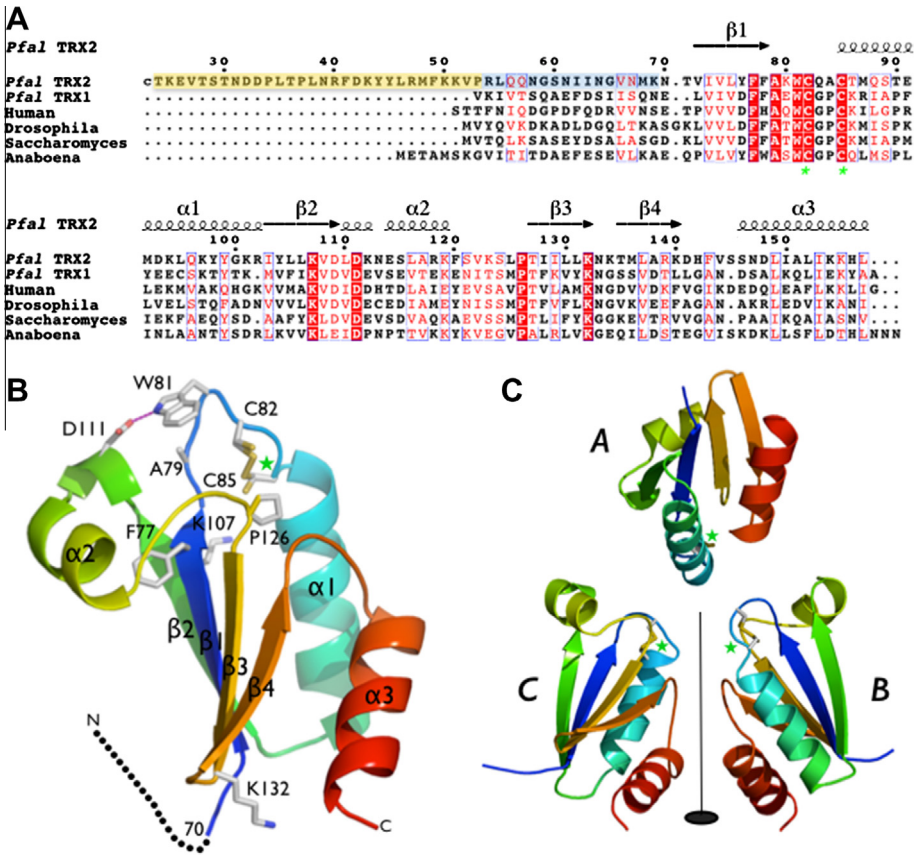

Fig. 1. General architecture of *Plasmodium* thioredoxin-2. (A) Structure-based sequence alignment of *Plasmodium* TRX2 against sequences of other thioredoxin proteins of known structure from human (1UVZ), *Drosophila* (1XWA), yeast (2FA4), *Anaboena* (1THX) and another thioredoxin from *Plasmodium* (1SYR). Secondary structure elements correspond to our structure. Residues T24-K69 (shaded in yellow) are not seen in our structure, residues R54-K69 (shaded in blue) were observed in a previously published structure [23]. (B) Crystal structure of TRX2 from *Plasmodium falciparum*. Secondary structure elements are labeled and colored using a rainbow pattern. Strictly conserved residues among thioredoxins, including the two catalytic cysteines (C82 and C85) and residues W81 and D111 involved in a stabilizing hydrogen bond, are labeled. Catalytic cysteines are shown in the two alternate conformations observed in the crystal corresponding to the reduced and the oxidized states (chains A and B). The missing and disordered N-terminal part of the chain is indicated as a dotted line. (C) Three chains of *Plasmodium* TRX2 are observed in the asymmetric unit. A 2-fold non-crystallographic symmetry operator relates chains B and C. The three N-termini point towards solvent-accessible openings of the crystalline lattice. (For interpretation of the references to color in this figure legend, the reader is referred to the web version of this article.)

computational approaches based on ligand docking and normal mode analysis. The protein adopts a canonical βαβαββα thioredoxin fold where the catalytic motif $C_{82}XXC_{85}$ sits in a solvent accessible loop between strand β1 and helix α1. The active site configuration is stabilized by a conserved hydrogen bond between the strictly conserved residues W81 and D111 (Fig. 1A and B). We built residues N70 through L157, the entire thioredoxin core domain, in our experimental electron density maps; some weak residual density probably corresponding to disordered parts of the remaining chain was observed. The asymmetric unit contains three monomers (Fig. 1C) whose N-termini point towards solvent-filled channels large enough to accommodate the missing residues. In our hands, full-length TRX2 was refractory to purification; despite the use of N-terminal fusion proteins, we observed a persistent N-terminal proteolytic cleavage. Mass spectrometry analysis reveals that the crystallized protein has molecular weights ranging from 12,381 to 13,268 Da and is thus longer than the polypeptide built in our electron density maps (10,777 Da) but still shorter than the expected 16,203 Da (data not shown).

The 2.9 Å resolution structure of *Plasmodium* TRX2 reported previously [23] (PDB: 3UL3) shows that the 16 extra N-terminal residues (backbone only for residues R54 through K69) can adopt an extended featureless conformation (Fig. 3A and Supplementary Fig. S2). A non-crystallographic 'pseudo-dimer' of TRX2 was present in the asymmetric unit; computational analysis however indicated that this dimer is unlikely to exist in solution. In contrast with the coiled-coil conformation observed in 3UL3, the variable N-terminal extensions of *Plasmodium* TRX1 and TRX3 and human mitochondrial TRX2 all fold as a α-helix packed against the four-stranded β sheet present in the thioredoxin fold (Supplementary Fig. S3). This suggests that the N-terminus of monomeric TRX2 is dynamic and samples several conformations.

3.2. Plasmodium thioredoxin-2 samples its two redox catalytic states in the crystal lattice

Thioredoxins are ubiquitous proteins that act as both reducing agents of small compounds and protein disulfide reductases. *Pfal*-TRX2 assists protein export by breaking disulfide bonds of parasitic proteins targeted for export, thus facilitating the ATP-dependent protein unfolding catalyzed by the AAA + protein HSP101/ClpB2. Within the asymmetric unit, the three independent copies of TRX2 are observed under different oxidation states (Figs. 1C and 2). Molecule C is fully oxidized with an intra-molecular disulfide bond (2.1 Å distance between sulfur atoms) refined at full occupancy between the two conserved catalytic cysteines C82 and C85 (Fig. 2A). On the other hand, in molecules A and B these two residues adopt alternate conformations with occupancies of 0.60 and 0.40 for the reduced and oxidized forms, respectively. Upon reduction, the two free thiol groups move 3.6 Å away (Fig. 2B). In our hands, it proved impossible to crystallize fully reduced TRX2. However, the structure from Sharma et al. corresponds to the fully reduced form, with a 3.8 Å sulfur-to-sulfur distance and a conformation similar to the one we observe for chains A and B in our crystal form.

Thioredoxins reduce other proteins by cysteine thiol-disulfide exchange. The thiol from residue C82 is likely to be the first nucleophile to attack disulfides from substrate proteins; the resulting inter-molecular disulfide link between TRX2 and its substrates is then attacked by the second nucleophilic thiol group from residue C85 to release its reduced substrate. Gold-based metallo-drugs behave as thiol and selenol reactive species. In particular, gold-I organo-metallic compounds such as auro-thiomalate and auro-thioglucose exhibit potent antimalarial effects *in vitro* and *in vivo* [33]. These two drugs are well-established treatments against

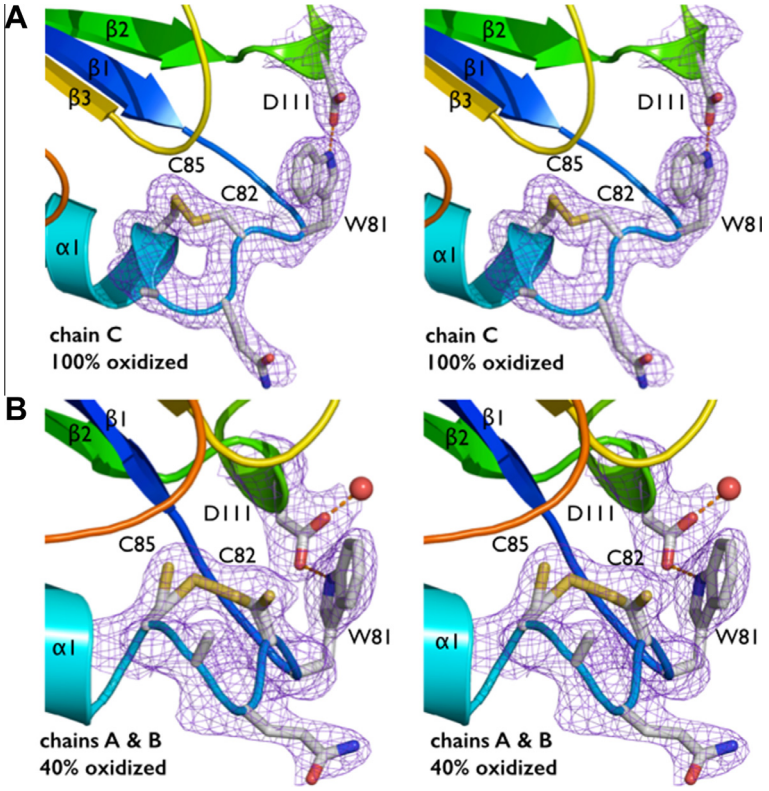

Fig. 2. *Plasmodium* thioredoxin-2 samples its two redox states in the crystal. 2m*Fo*-D*Fc* Fourier difference electron density maps contoured at 1.5σ showing the catalytic pair of cysteines of *Pfal*-TRX2 observed in different oxidation states. (A) 100% oxidized form in chain C and (B) 40% oxidized /60% reduced forms in chains A and B. Complete oxidation results in the formation of an intra-molecular disulfide bond. The stabilizing hydrogen bond between conserved residues W81 and D111 is shown.

rheumatoid arthritis and were characterized as potential anti-trypanosomial and anti-leishmanial agents [34]. They are known inhibitors of thioredoxin reductase, the enzyme that regenerates thioredoxin into its fully reduced form. In the leishmanial trypanothione reductase [35] and the schistosomal thioredoxin–glutatione reductase [36], gold binds to and bridges the two active-site cysteine residues that are 3.5–4.5 Å apart. Auro-thiomalate also inhibits *Plasmodium* TRX2 [23]; the strongly thiophilic gold atom is likely to interact with the two SH groups of the $C_{82}XXC_{85}$ catalytic motif of TRX2 in a similar way.

3.3. Conformations of the Plasmodium TRX2 in solution

We characterized the association state and conformation of *Pfal*-TRX2 in solution using SAXS [37]. The Kratky plot indicates that the protein is folded in solution and overall compact (Fig. 3A). We derived the experimental value of its radius of gyration (R_G) values by Guinier analysis (Table S1 and Fig. 3B). Experimental scattering curves were fitted against theoretical curves calculated using our crystal structures (Fig. 3C and Supplementary Figs. S3 and S4). Pair distance distribution functions ($P(r)$) estimated by Fourier inversion of the experimental intensities were compared to those calculated from atomic models and used to estimate D_{max} (the longest intra-molecular distance) and R_G values independent of the Guinier analysis (Supplementary Table S1 and Fig. 3D).

The experimental R_G = 16.1 Å of *Pfal*-TRX2 is quite different from the 14.1 Å value derived from our X-ray structure (PDB 4O32). Attempts to fit experimental data against the theoretical scattering curve calculated from our crystal structure result in a poor fit (χ^2 = 2.347) indicating a significant deviation between our model and the average conformation in solution. However, we also fitted our data using the monomer and the pseudo-dimer models of TRX2 described in the previously reported crystal structure [23] (PDB 3UL3) (Supplementary Figs. S3 and S4) where the refined model is longer by 16 amino acids at its N-terminus. Not surprisingly, attempts to model our solution scattering data using the crystallographic pseudo-dimer also result in a very poor fit (χ^2 = 6.470). However, the fit (χ^2 = 1.089) obtained using the monomer with this longer N-terminal extension indicates that the solution conformation resembles more closely this structure. The non-conserved N-terminal extension of *Plasmodium* TRX2 may also sample other conformations; however, the fit of our data against a homology model where the 20 residues preceding the thioredoxin core are modeled in the α-helical conformation observed in other thioredoxins (Supplementary Figs. S3 and S4),

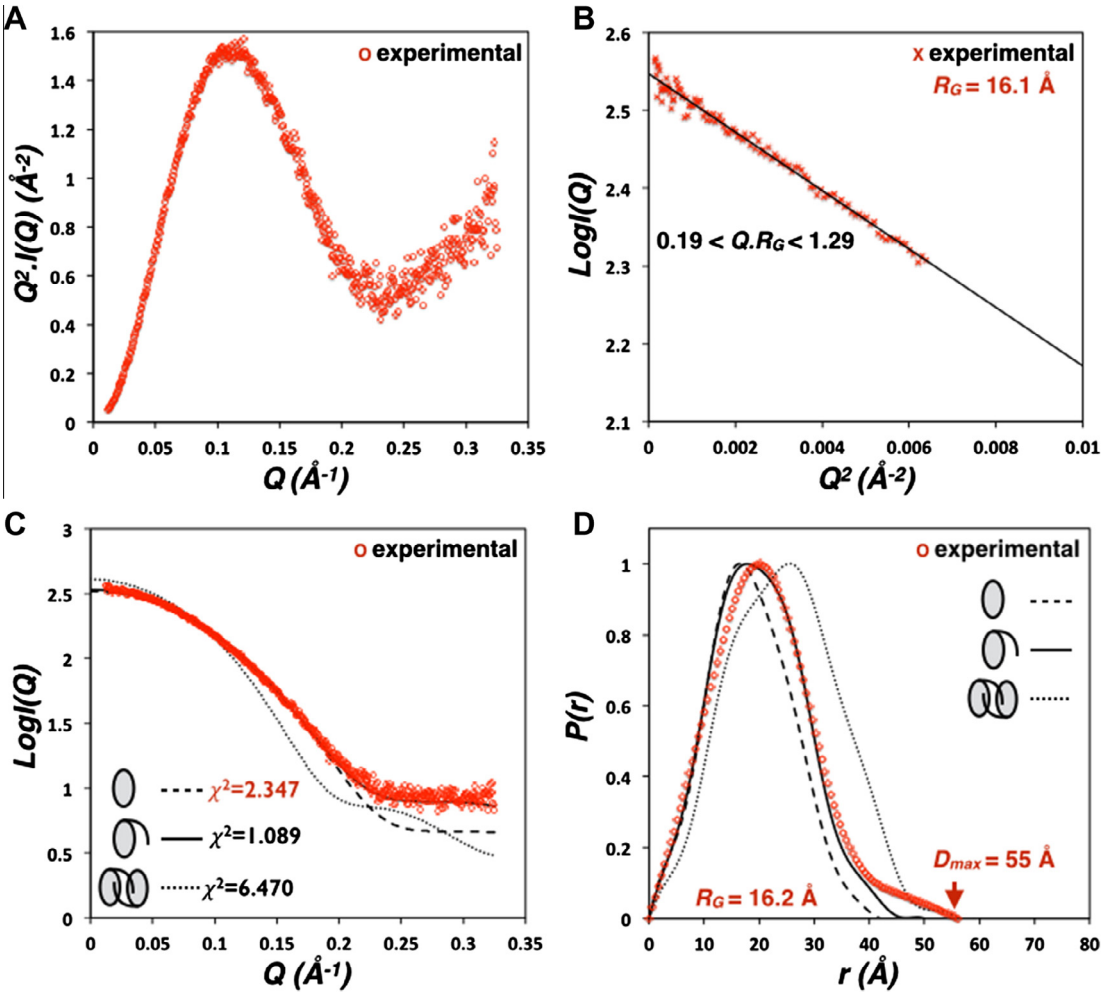

Fig. 3. Solution characterization of *Plasmodium* thioredoxin-2 by SAXS. (A) Kratky plot showing that *Pfal*-TRX2 is folded in solution. (B) Guinier plot shown with the corresponding experimental value of the radius of gyration. Guinier's law was applied is in its most conservative form for a QR_G angular range not exceeding 1.3. (C) Scattering curve fits. Experimental curves (red) fitted against curves calculated from the X-ray structures (black). The discrepancy factor for each fit is indicated. (D) Pair distance distribution functions. Experimental curves (red) and curves calculated from the X-ray structures of the three models (black) with *GNOM*. D_{max} and R_G experimental values are indicated. (For interpretation of the references to color in this figure legend, the reader is referred to the web version of this article.)

is also of poor quality (χ^2 = 3.046). Interestingly, $P(r)$ distributions analysis still show some discrepancy between the N-terminal extended (best) model and our experimental data; this is likely the result of a greater conformational flexibility and a slightly longer N-terminal extension than the one reported in structure 3UL3. Altogether, our SAXS data demonstrate that *Plasmodium* TRX2 is monomeric in solution, in agreement with the SEC analysis (Supplementary Fig. S2B).

The high-resolution crystal structure of the vacuolar thioredoxin-2 from the malaria parasite provides us with a necessary template to model the binding of small molecules and identify pharmacophores to guide the rational design of novel antimalarials.

Accession number

The coordinates and structure factors have been deposited into the Protein Data Bank, under the accession PDB code: 4O32.

Acknowledgments

This work was supported by the UCLA David Geffen School of Medicine, the UCLA Scholars in Translational Medicine Program Award, the Alexander and Renée Kolin Endowed Professorship in Molecular Biology and Biophysics and the National Center for Advancing Translational Sciences UCLA CTSI Grant UL1TR000124 to PFE. We thank the staffs of the NECAT beamline 24-ID (APS, Chicago) and of the SYBILS beamline 12.3.1 (ALS, Berkeley) for their expertise and assistance.

Appendix A. Supplementary data

Supplementary data associated with this article can be found, in the online version, at http://dx.doi.org/10.1016/j.bbrc.2014.11.096.

References

[1] P.L. Olliaro, W.R. Taylor, Antimalarial compounds: from bench to bedside, J. Exp. Biol. 206 (2003) 3753–3759.
[2] J.G. Waterkeyn, M.E. Wickham, K.M. Davern, B.M. Cooke, R.L. Coppel, J.C. Reeder, J.G. Culvenor, R.F. Waller, A.F. Cowman, Targeted mutagenesis of *Plasmodium falciparum* erythrocyte membrane protein 3 (PfEMP3) disrupts cytoadherence of malaria-infected red blood cells, EMBO J. 19 (2000) 2813–2823.
[3] A.G. Maier, M. Rug, M.T. O'Neill, M. Brown, S. Chakravorty, T. Szestak, J. Chesson, Y. Wu, K. Hughes, R.L. Coppel, C. Newbold, J.G. Beeson, A. Craig, B.S. Crabb, A.F. Cowman, Exported proteins required for virulence and rigidity of *Plasmodium falciparum*-infected human erythrocytes, Cell 134 (2008) 48–61.
[4] B.S. Crabb, B.M. Cooke, J.C. Reeder, R.F. Waller, S.R. Caruana, K.M. Davern, M.E. Wickham, G.V. Brown, R.L. Coppel, A.F. Cowman, Targeted gene disruption shows that knobs enable malaria-infected red cells to cytoadhere under physiological shear stress, Cell 89 (1997) 287–296.
[5] T.F. de Koning-Ward, P.R. Gilson, J.A. Boddey, M. Rug, B.J. Smith, A.T. Papenfuss, P.R. Sanders, R.J. Lundie, A.G. Maier, A.F. Cowman, B.S. Crabb, A newly discovered protein export machine in malaria parasites, Nature 459 (2009) 945–949.
[6] H.E. Bullen, S.C. Charnaud, M. Kalanon, D.T. Riglar, C. Dekiwadia, N. Kangwanrangsan, M. Torii, T. Tsuboi, J. Baum, S.A. Ralph, A.F. Cowman, T.F. de Koning-Ward, B.S. Crabb, P.R. Gilson, Biosynthesis, localisation and macromolecular arrangement of the *Plasmodium falciparum* translocon of exported proteins; PTEX, J. Biol. Chem. 287 (2012) 7871–7884.
[7] K. Fischer, T. Marti, B. Rick, D. Johnson, J. Benting, S. Baumeister, C. Helmbrecht, M. Lanzer, K. Lingelbach, Characterization and cloning of the gene encoding the vacuolar membrane protein EXP-2 from *Plasmodium falciparum*, Mol. Biochem. Parasitol. 92 (1998) 47–57.
[8] D.T. Riglar, K.L. Rogers, E. Hanssen, L. Turnbull, H.E. Bullen, S.C. Charnaud, J. Przyborski, P.R. Gilson, C.B. Whitchurch, B.S. Crabb, J. Baum, A.F. Cowman, Spatial association with PTEX complexes defines regions for effector export into *Plasmodium falciparum*-infected erythrocytes, Nat. Commun. 4 (2013) 1415.
[9] A.J. Wallace, T.J. Stillman, A. Atkins, S.J. Jamieson, P.A. Bullough, J. Green, P.J. Artymiuk, *E coli* hemolysin E (HlyE, ClyA, SheA): X-ray crystal structure of the toxin and observation of membrane pores by electron microscopy, Cell 100 (2000) 265–276.
[10] N. Eifler, M. Vetsch, M. Gregorini, P. Ringler, M. Chami, A. Philippsen, A. Fritz, S.A. Muller, R. Glockshuber, A. Engel, U. Grauschopf, Cytotoxin ClyA from *Escherichia coli* assembles to a 13-meric pore independent of its redox-state, EMBO J. 25 (2006) 2652–2661.
[11] M. Mueller, U. Grauschopf, T. Maier, R. Glockshuber, N. Ban, The structure of a cytolytic alpha-helical toxin pore reveals its assembly mechanism, Nature 459 (2009) 726–730.
[12] N.L. Hiller, S. Bhattacharjee, C. van Ooij, K. Liolios, T. Harrison, C. Lopez-Estrano, K. Haldar, A host-targeting signal in virulence proteins reveals a secretome in malarial infection, Science 306 (2004) 1934–1937.
[13] M. Marti, R.T. Good, M. Rug, E. Knuepfer, A.F. Cowman, Targeting malaria virulence and remodeling proteins to the host erythrocyte, Science 306 (2004) 1930–1933.
[14] I. Russo, S. Babbitt, V. Muralidharan, T. Butler, A. Oksman, D.E. Goldberg, Plasmepsin V licenses *Plasmodium* proteins for export into the host erythrocyte, Nature 463 (2010) 632–636.
[15] J.A. Boddey, A.N. Hodder, S. Gunther, P.R. Gilson, H. Patsiouras, E.A. Kapp, J.A. Pearce, T.F. de Koning-Ward, R.J. Simpson, B.S. Crabb, A.F. Cowman, An aspartyl protease directs malaria effector proteins to the host cell, Nature 463 (2010) 627–631.
[16] N. Gehde, C. Hinrichs, I. Montilla, S. Charpian, K. Lingelbach, J.M. Przyborski, Protein unfolding is an essential requirement for transport across the parasitophorous vacuolar membrane of *Plasmodium falciparum*, Mol. Microbiol. 71 (2009) 613–628.
[17] M. El Bakkouri, A. Pow, A. Mulichak, K.L. Cheung, J.D. Artz, M. Amani, S. Fell, T.F. de Koning-Ward, C.D. Goodman, G.I. McFadden, J. Ortega, R. Hui, W.A. Houry, The Clp chaperones and proteases of the human malaria parasite *Plasmodium falciparum*, J. Mol. Biol. 404 (2010) 456–477.
[18] J.R. Beck, V. Muralidharan, A. Oksman, D.E. Goldberg, PTEX component HSP101 mediates export of diverse malaria effectors into host erythrocytes, Nature 511 (2014) 592–595.
[19] B. Elsworth, K. Matthews, C.Q. Nie, M. Kalanon, S.C. Charnaud, P.R. Sanders, S.A. Chisholm, N.A. Counihan, P.J. Shaw, P. Pino, J.A. Chan, M.F. Azevedo, S.J. Rogerson, J.G. Beeson, B.S. Crabb, P.R. Gilson, T.F. de Koning-Ward, PTEX is an essential nexus for protein export in malaria parasites, Nature 511 (2014) 587–591.
[20] K. Matthews, M. Kalanon, S.A. Chisholm, A. Sturm, C.D. Goodman, M.W. Dixon, P.R. Sanders, T. Nebl, F. Fraser, S. Haase, G.I. McFadden, P.R. Gilson, B.S. Crabb, T.F. de Koning-Ward, The *Plasmodium* translocon of exported proteins (PTEX) component thioredoxin-2 is important for maintaining normal blood-stage growth, Mol. Microbiol. 89 (2013) 1167–1186.
[21] J.M. Matz, K. Matuschewski, T.W. Kooij, Two putative protein export regulators promote *Plasmodium* blood stage development in vivo, Mol. Biochem. Parasitol. 191 (2013) 44–52.
[22] I. Martin, J. Underhaug, G. Celaya, F. Moro, K. Teigen, A. Martinez, A. Muga, Screening and evaluation of small organic molecules as ClpB inhibitors and potential antimicrobials, J. Med. Chem. 56 (2013) 7177–7189.
[23] A. Sharma, S. Dixit, Structural insights into thioredoxin-2: a component of malaria parasite protein secretion machinery, Sci. Rep. 1 (2011) 179.
[24] S. Doublie, Preparation of selenomethionyl proteins for phase determination, Methods Enzymol. 276 (1997) 523–530.
[25] W. Kabsch, Xds, Acta Crystallogr. D Biol. Crystallogr. 66 (2010) 125–132.
[26] P. Emsley, K. Cowtan, Coot: model-building tools for molecular graphics, Acta Crystallogr. D Biol. Crystallogr. 60 (2004) 2126–2132.
[27] P.D. Adams, P.V. Afonine, G. Bunkoczi, V.B. Chen, I.W. Davis, N. Echols, J.J. Headd, L.W. Hung, G.J. Kapral, R.W. Grosse-Kunstleve, A.J. McCoy, N.W. Moriarty, R. Oeffner, R.J. Read, D.C. Richardson, J.S. Richardson, T.C. Terwilliger, P.H. Zwart, PHENIX: a comprehensive Python-based system for macromolecular structure solution, Acta Crystallogr. D Biol. Crystallogr. 66 (2010) 213–221.
[28] S. Classen, G.L. Hura, J.M. Holton, R.P. Rambo, I. Rodic, P.J. McGuire, K. Dyer, M. Hammel, G. Meigs, K.A. Frankel, J.A. Tainer, Implementation and performance of SIBYLS: a dual endstation small-angle X-ray scattering and macromolecular crystallography beamline at the Advanced Light Source, J. Appl. Crystallogr. 46 (2013) 1–13.
[29] G.L. Hura, A.L. Menon, M. Hammel, R.P. Rambo, F.L. Poole 2nd, S.E. Tsutakawa, F.E. Jenney Jr., S. Classen, K.A. Frankel, R.C. Hopkins, S.J. Yang, J.W. Scott, B.D. Dillard, M.W. Adams, J.A. Tainer, Robust, high-throughput solution structural analyses by small angle X-ray scattering (SAXS), Nat. Methods 6 (2009) 606–612.
[30] R.P. Rambo, J.A. Tainer, Characterizing flexible and intrinsically unstructured biological macromolecules by SAS using the Porod-Debye law, Biopolymers 95 (2011) 559–571.
[31] D.I. Svergun, C. Barberato, M.H. Koch, CRYSOL: a program to evaluate X-ray solution scattering of biological macromolecules from atomic coordinates, J. Appl. Crystallogr. 28 (1995) 768–773.
[32] D.I. Svergun, Determination of the regularization parameter in indirect transform methods using perceptual criteria, J. Appl. Crystallogr. 25 (1992) 495–503.
[33] A.R. Sannella, A. Casini, C. Gabbiani, L. Messori, A.R. Bilia, F.F. Vincieri, G. Majori, C. Severini, New uses for old drugs. Auranofin, a clinically established antiarthritic metallodrug, exhibits potent antimalarial effects in vitro: Mechanistic and pharmacological implications, FEBS Lett. 582 (2008) 844–847.
[34] G. Colotti, A. Ilari, A. Fiorillo, P. Baiocco, M.A. Cinellu, L. Maiore, F. Scaletti, C. Gabbiani, L. Messori, Metal-based compounds as prospective antileishmanial

agents: inhibition of trypanothione reductase by selected gold complexes, ChemMedChem (2013).
[35] A. Ilari, P. Baiocco, L. Messori, A. Fiorillo, A. Boffi, M. Gramiccia, T. Di Muccio, G. Colotti, A gold-containing drug against parasitic polyamine metabolism: the X-ray structure of trypanothione reductase from *Leishmania infantum* in complex with auranofin reveals a dual mechanism of enzyme inhibition, Amino Acids 42 (2012) 803–811.
[36] F. Angelucci, A.A. Sayed, D.L. Williams, G. Boumis, M. Brunori, D. Dimastrogiovanni, A.E. Miele, F. Pauly, A. Bellelli, Inhibition of *Schistosoma mansoni* thioredoxin–glutathione reductase by auranofin: structural and kinetic aspects, J. Biol. Chem. 284 (2009) 28977–28985.
[37] C.E. Blanchet, D.I. Svergun, Small-angle X-ray scattering on biological macromolecules and nanocomposites in solution, Annu. Rev. Phys. Chem. 64 (2013) 37–54.
[38] K. Diederichs, P.A. Karplus, Improved R-factors for diffraction data analysis in macromolecular crystallography, Nat Struct Biol 4 (1997) 269–275.
[39] P.A. Karplus, K. Diederichs, Linking crystallographic model and data quality, Science 336 (2012) 1030–1033.